Significance of Quenching Stress in the Cohesion and Adhesion of Thermally Sprayed Coatings

S. Kuroda, T. Fukushima, and S. Kitahara

In thermal spraying, molten particles strike a solid surface, where they are flattened and quenched within a very short time. Considerable in-plane tensile stress on the order of 100 MPa can develop within each splat during quenching after solidification because thermal contraction of the particle is constrained by the underlying solid. Ni-20Cr alloy and alumina powders have been plasma sprayed in air onto steel substrates that were maintained at about 473 K. The influence of spraying conditions such as spray distance on the magnitude of the quenching stress have been studied by measuring the curvature of the substrate during spraying. Mechanical properties such as Young's modulus and bend strength of the deposited coatings have also been measured. A strong correlation was found between the quenching stress and the strength of Ni-20Cr coatings, which suggests that the strength of interlamellar bonding limits the quenching stress at such temperature.

1. Introduction

In thermal spraying, molten particles strike a solid surface, where they are flattened and quenched within a few microseconds. Even though this process of splat quenching is the fundamental mechanism of building up sprayed coatings, it is difficult to observe this phenomenon directly because it is not only a microscopic but also a very fast process. Recent studies have revealed that a high level of in-plane tensile stress (on the order of 100 MPa) can develop within each splat during quenching after solidification because thermal contraction of the splat is constrained by the underlying solid, as schematically shown in Fig. 1.[1,2] Understanding and evaluation of quenching stress is essential for prediction of residual stresses in sprayed coatings and other related applications.[3-5] The quenching stress (σ_q) has been measured for various combinations of spray and substrate materials, and it has been shown that the stress is independent of the substrate material. Effects of the substrate material and surface pretreatment on the quenching stress exist only for a very limited region near the coating/substrate interface, which is less than 10 μm in terms of coating thickness.[6]

However, the stress of each spray material has a distinct dependence on the substrate temperature, T_s. For example, Fig. 2 shows the measured dependence of σ_q for nickel, Ni-20Cr alloy, and alumina on the homologous substrate temperature T_s/T_m, where T_m is the melting point of each spray material.[1] If bonding was perfect between a splat and the underlying solid, a stress higher than the yield stress of each spray material could be expected within such a thin plate. In reality, however, this is not the case, and the measured stress values are much lower. Therefore, various stress relaxation mechanisms have been suggested to

Key Words: fracture morphology, mechanical properties, quenching stress, residual stress, Young's modulus

S. Kuroda, T. Fukushima, and **S. Kitahara,** National Research Institute for Metals, Advanced Materials Processing Division, Tokyo, Japan. Presented at ITSC '92, June, 1992, Orlando, Florida.

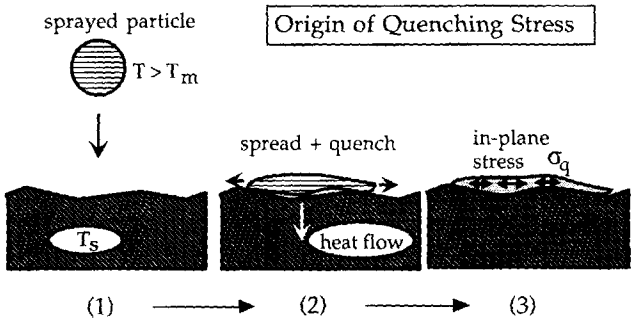

Figure 1 Origin of quenching stress in thermal spraying.

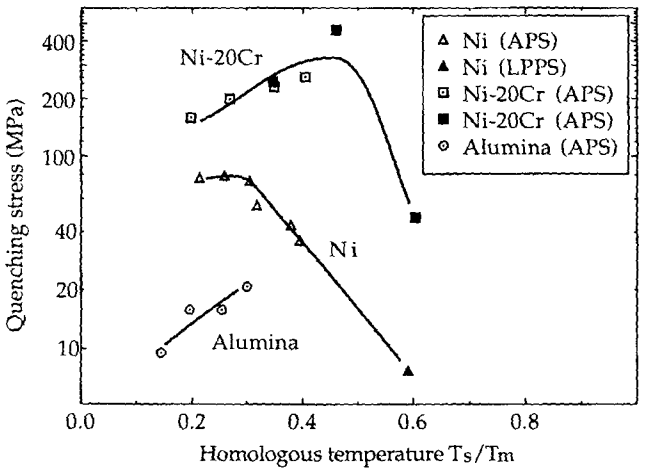

Figure 2 Measured values of the quenching stress for nickel, Ni-20Cr alloy, and alumina plotted against homologous temperature (T_s/T_m).[1] T_s is the substrate temperature, and T_m is the melting point of each spray material. APS: atmospheric plasma spray, LPPS: low pressure plasma spray.

Table 1 Typical Spray Conditions

Powder	Plasma gas/flow rate, l/min	Arc current/voltage	Powder feed rate, g/min	Powder feed gas flow rate, l/min
Ni-20Cr	Ar, 45	750A, 30V	10	2.5
Al_2O_3	Ar, 45	750A, 30V	5	2.5

Note: Torch linear velocity in front of a substrate: 0.18 m/s.

operate during quenching. Based on the observed temperature dependence of σ_q and structural observation of deposits, the major stress relaxation mechanisms are likely to be yielding and creep for metallic splats and microcracking for ceramic splats. The generally high level of σ_q in sprayed Ni-20Cr compared to pure nickel can be understood in the light of its higher yield strength and resistance to creep. For ceramic materials, microcracking is believed to reduce the quenching stress to a much lower level compared to metals.

A clear positive dependence of σ_q on T_s in the lower temperature range has been observed for materials such as Ni-20Cr and alumina as well as molybdenum, NiCrAlY, and zirconia.[1] It has been postulated that this is due to the change in the bonding between splats. When a sprayed particle is quenched, the degree of constraint against thermal contraction depends on how tightly the particle is bonded to the underlying solid, *i.e.*, the previously formed deposit. If the bonding is loose, then interfacial sliding could take place to reduce the final stress within the splat. Because the elastic modulus of coatings formed on a substrate at higher temperature is higher than those formed at a lower temperature, it seems that the bonding between splats is "better" for coatings formed at higher T_s values. Thus, σ_q increases with T_s until other stress relaxation mechanisms such as plastic yielding and creep become effective.

Because one of the major advantages of thermal spraying is that it can apply surface coatings without excessively heating substrates, it is important to understand the nature of stress generation in the low-temperature range, especially for the atmospheric plasma spray (APS) process. Therefore, the present work further tests the latest supposition by examining the dependence of σ_q on another important spray parameter, *i.e.*, spray distance, in the low T_s range. Ni-20Cr and alumina were chosen as model materials due to their contrasting stress behavior. Relationships between the characteristics of the impinging powders, namely temperature and velocity, and σ_q, as well as other mechanical properties such as the elastic modulus and fracture stress of deposits, will be discussed with some structural observations of splats and fracture surfaces.

2. Experiments

Commercially available Ni-20Cr alloy and alumina powders with a 10- to 45-μm size distribution were plasma sprayed in air using an 80-kW torch under the conditions listed in Table 1.

2.1 *Measurement of Temperature and Velocity of Sprayed Particles*

Velocity and surface temperature of sprayed particles in flight were measured by optical methods based on spatial filtering and color pyrometry.[7] Thermal radiation emitted by a sprayed particle was transmitted through a number of equally spaced slits to be converted to an electrical current by a photomultiplier. When a particle travels in front of the slits, oscillations appear in the current signal, whose frequency is proportional to the particle velocity. During temperature measurement, the spectrum of the thermal radiation was analyzed by a monochromator and compared with the spectra of black body radiation to find the temperature that provides the best fit to the observed spectrum. For a stream of sprayed particles, two-dimensional intensity distribution of radiation in the plane containing the direction of powder injection was measured first, and a trajectory, along which the vertical intensity distribution was at its maximum, was determined. The following measurements of velocity and temperature at various spray distances were made along this "brightest trajectory," which can be regarded as the core of the stream of sprayed particles.

2.2 *Measurement of Deposition Efficiency*

Deposition efficiency was measured by spraying onto a 100 by 100 mm steel plate substrate that was maintained at around 473 K during the spraying process. By scanning the spraying torch with velocity (v) transversely over the substrate with width (B) for n times during a period (t) and measuring the weight gain (ΔW) of the substrate and the weight (w) of the powder consumed during the run, the deposition efficiency η was given by:

$$\eta = \frac{\Delta W}{w} \times \frac{vt}{nB} \quad [1]$$

The factor vt/nB is included to take into account the loss of powder by overspraying. The width of a scan was set wider than the substrate width. Thus, the torch was not directed onto the substrate, when it was stopped after each scan to prevent the substrate from overheating.

2.3 *Measurement of Quenching Stress*

Suppose a thin film were stretched and then its surface were bonded to a substrate, the substrate would bend, and the film/substrate couple would come to an equilibrium. If the film thickness is negligible with respect to the substrate thickness, the equilibrium curvature of the substrate is proportional to the stress within the film.[8] The following technique is based on this principle. The curvature of a substrate was measured *in situ* during spraying by the instrument shown in Fig. 3, the details of which have been reported elsewhere.[9] The instrument detects the bending (δ) of a substrate fixed onto a pair of knife edges by a contacting displacement sensor (DS). The parameter δ is proportional to the curvature $1/R$ of the substrate. The substrate was a 2 by 15 by 100 mm mild steel plate, which was alumina grit

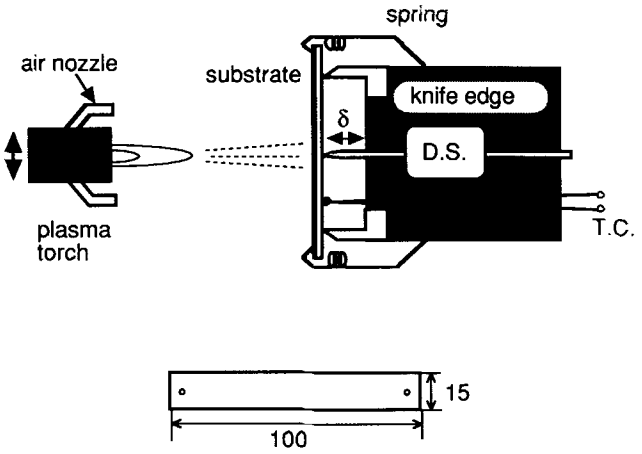

Figure 3 Schematic of the *in situ* instrument to measure the curvature change of a substrate during spraying.

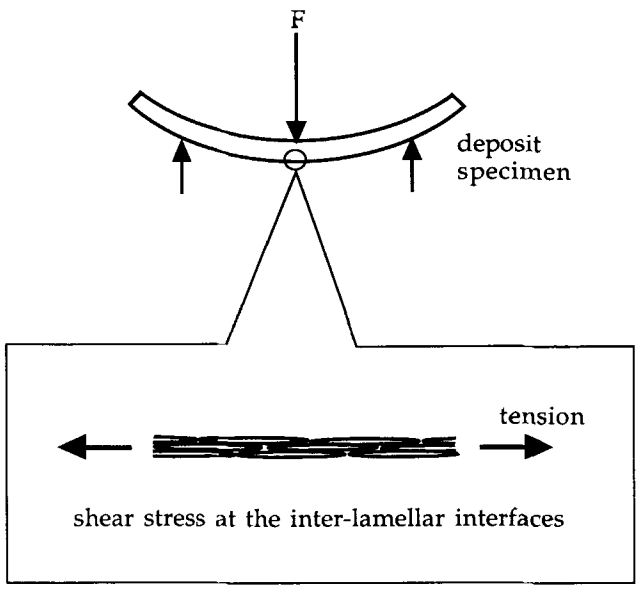

Figure 4 Schematic of three-point bending and the stress state at the bottom surface of a specimen. The section is in tension as a continuum, but a shear stress is acting at the interlamellar interfaces.

blasted and degreased before spraying. The tension exerted by a pair of springs used to fix the substrate causes only a few microns of δ, which is negligible in most cases. Within such a thin substrate, no significant stationary thermal gradient in the thickness direction exists during spraying, and thus, the curvature may be regarded as a direct measure of the quenching stress within the deposited coating as long as the average substrate temperature (T_s) is kept constant.[6] The temperature of the substrate was measured by a thermocouple that was spot welded to the rear surface and was controlled to a target temperature of around 473 K by adjusting the flow rate of the cooling air ejected by a pair of nozzles attached to the plasma torch. The torch traverses back and forth in front of the substrate at a velocity of 0.18 m/s, with a small up or down motion at the end of each traverse to form a coating of uniform thickness. From the rate of the curvature change with respect to the coating thickness (h_d), the average quenching stress, $\sigma_q(T_s)$, within splats can be determined as:

$$\sigma_q(T_s) = \frac{E_s(T_s)h_s^2}{6(1-\nu)} \frac{\partial}{\partial h_d}\left(\frac{1}{R}\right) \qquad [2]$$

where E_s, h_s, and ν are the Young's modulus, thickness, and Poisson's ratio of the substrate, respectively.[9-11]

2.4 *Mechanical Properties*

A three-point bending test was used to measure the Young's modulus and the strength of deposits that were stripped from the substrate. For specimen preparation, deposits formed during the curvature measurement were used. As shown below, it is possible to detect the onset of failure at the coating/substrate interface during spraying by using the *in situ* curvature instrument. These coatings could be easily detached from the substrate after further build-up of the deposit. In some cases, silicone-base liquid was sprayed on a substrate before deposition to enhance separation of a coating from the substrate. In the case of nickel-chromium deposits, one coating was cut into four pieces of 7 by 50 mm by a fine cutting wheel. For alumina deposits, no such cutting was done to prevent introduction of cracks. The thickness of specimens ranged from 0.5 to 1.7 mm.

As shown schematically in Fig. 4, the section at the top surface of a specimen is in the highest tension, where a crack is most likely to be initiated. When viewed microscopically, however, a shear stress is acting on the interlamellar interfaces, which are probably the weakest links in the material. The load (F) at which the specimen fractured was measured and the fracture stress (σ_f) of the specimen was given by:

$$\sigma_f = \frac{FL}{4I}\left(\frac{h_d}{2}\right) \qquad [3]$$

where L is the span of the supports (40 mm), and I is the moment of inertia of the specimen cross section about an axis through its centroid. Because most specimens had a slight variation in thickness across their width (10% at maximum), the maximum distance between the surface and the neutral axis of the cross section was used instead of $h_d/2$ in the above equation.

3. Results and Discussion

3.1 *Velocity and Temperature of Sprayed Particles and Deposition Efficiency*

Figure 5 shows the change in the velocity (a) and temperature (b) of sprayed particles with respect to the spray distance, z. It is evident that alumina particles exhibit much steeper deceleration and cooling behavior with respect to z. Figure 6 shows the dependence of deposition efficiency on z. Whereas the nickel-chromium alloy shows a deposition efficiency over 60% for most of z, that of alumina is generally lower and is more sensi-

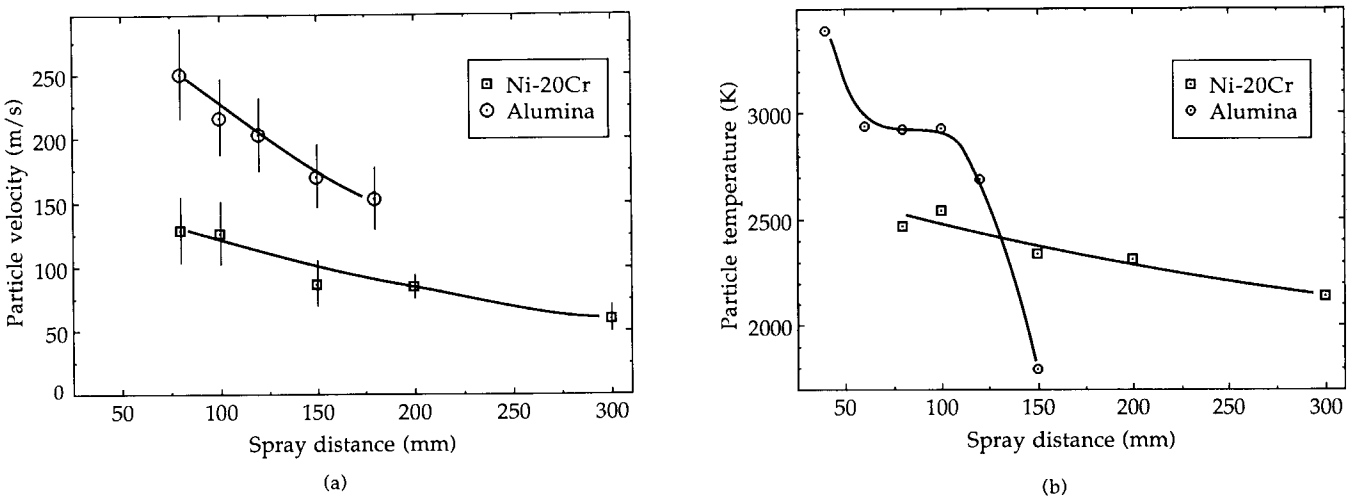

Figure 5 Change of velocity (**a**) and surface temperature (**b**) of sprayed particles with respect to the spray distance.

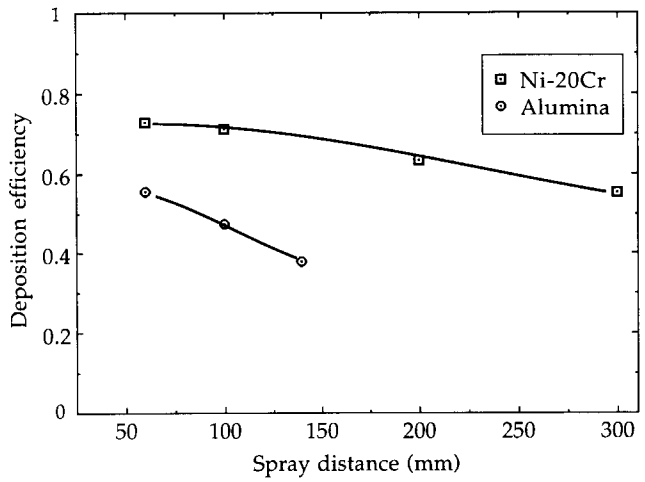

Figure 6 Variations in deposition efficiency with spray distance.

tive with respect to z. This fact agrees with the tendency observed in the temperature and velocity of sprayed particles shown in Fig. 5. For z over 140 mm, the deposition efficiency of alumina with the present electrical power input is so low that coating formation seems almost impractical. Based on these observations, the range of z for further experiments was determined to be from 60 to 300 mm for Ni-20Cr and from 60 to 140 mm for alumina.

Figure 7 shows scanning electron micrographs (SEM) of sprayed splats on polished stainless steel at $T_s \cong 473$ K. For Ni-20Cr, splats obtained at $z = 100$ mm (Fig. 7a) show the form of a flat disk with fine threads and particles at the periphery, apparently formed due to disintegration during spreading. In addition to these features, splats at $z = 300$ mm (Fig. 7b) show cracks in the surface oxide layer. For alumina, splats formed at $z = 60$ mm (Fig. 7c) exhibit heavy cracking, particularly in the region where splats overlap each other. Splats formed at $z = 140$ mm (Fig. 7d) exhibit few cracks and a lower degree of flattening compared to Fig. 7(c). This is probably because of the lower velocity of particles at impact, as well as the lower temperature, which results in a higher viscosity for molten alumina.

3.2 *Young's Modulus and Strength*

Figure 8 shows the change in the Young's modulus of sprayed coatings with the spray distance, z. Each plot represents results obtained from eight specimens in terms of the average and the standard deviation. The solid plots are from deposits made onto substrates held at a higher temperature of around 800 K. The arrows indicate the relative magnitudes of the measured modulus to the handbook bulk E_o values of the materials (E_o = 214 GPa for Ni-20Cr and 370 GPa for alumina). Even though the sprayed alumina is predominantly composed of metastable γ phase, the E value of sintered α-alumina is presented. The value of γ- alumina is not known, but is estimated to be somewhat lower than that of α-alumina.[12] The modulus of metallic deposits sprayed onto such a relatively low-temperature substrate is generally about one third of the bulk, whereas that of ceramic deposits is usually much lower.[1,12]

In a previous work, the Eshelby equivalent homogeneous inclusion model, which treats porosity as randomly distributed ellipsoids with zero stiffness, was used to examine the effects of pores on the modulus of sprayed deposits.[1] The model assumes that the matrix is a solid body and suggests that very thin plate-shaped pores resembling through-thickness cracks perpendicular to the direction of applied stress are needed to reduce the modulus of a porous material to the observed extent where the porosity is around 10%. Globular pores cannot reduce the modulus to the observed extent. Because existence of such thin plate-shaped pores is unrealistic with materials like Ni-20Cr, poor bonding between lamellae was postulated[1] to be mainly responsible for the reduction in the stiffness of the metallic deposits.

The present results indicate that the modulus of alumina deposits changes more dramatically with respect to z compared to nickel-chromium deposits. Even though microcracks such as

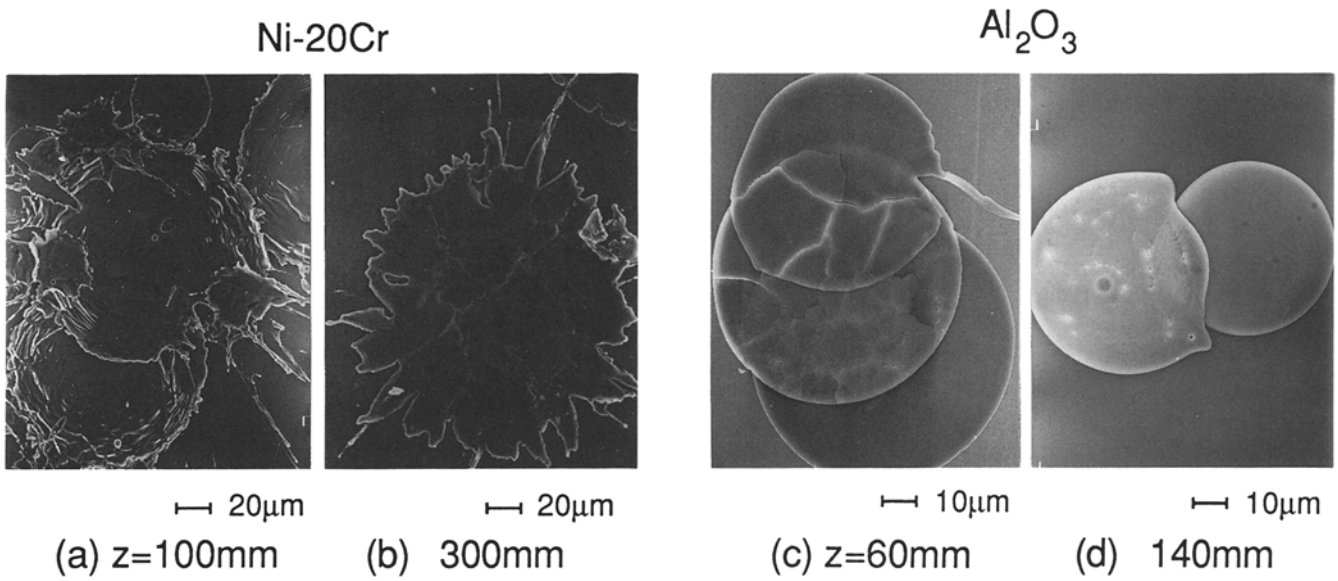

Figure 7 SEM observation of sprayed splats on polished stainless substrates placed at various distances. Ni-20Cr: **(a)** z = 100 mm, **(b)** 300 mm. Alumina: **(c)** z = 60 mm, **(d)** 140 mm.

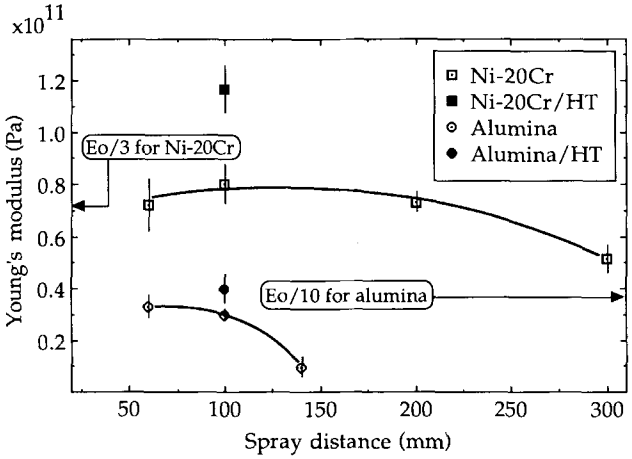

Figure 8 Variations in Young's modulus of sprayed deposits with spray distance. Average and standard deviation of eight specimens for each plot are shown.

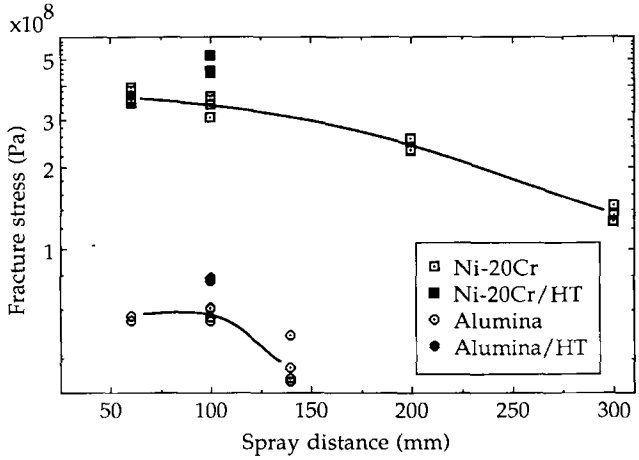

Figure 9 Variations in fracture stress of sprayed deposits with spray distance.

those evident in Fig. 7(c) are an obvious reason for the reduction of modulus in sprayed alumina compared to the bulk material and fit with the suggestion by the Eshelby model as mentioned above, microcracks in splats do not seem to increase with z, as shown in Fig. 7(d). Recently, some deliberate structural examinations of the interlamellar interface of alumina deposits have been performed. One approach uses TEM[12] and the other exploits electroplating alumina deposits with copper to fill pores and cracks with the metal and make them visible under SEM.[13] Both these works have shown that the real area of contact between lamellae is only 25 to 30% of the apparent area. It was also shown that the fraction of true contact between alumina lamellae increases with the electrical power input to the plasma torch.[13] The effect of an increase in spray distance is similar to that of a decrease in the power input to the torch because they both reduce the velocity and temperature of sprayed particles on impact against the substrate. It is likely, therefore, that the fraction of true contact between lamellae decreased with z in the present results and contributed largely to the observed reduction in the modulus of the alumina deposits with z.

In the bending tests, all the specimens fractured with a slight nonelastic deformation before failure. Figure 9 shows that the fracture stress exhibits a similar tendency to the modulus data. Figure 10 shows typical fracture surfaces observed under SEM. Ni-20Cr deposits at z = 100 mm (Fig. 10a) show a tightly overlaid lamellar structure, whereas such a structure is less obvious in Fig. 10(b) formed at z = 300 mm, where pores a few micrometers in size are evident. Fracture surfaces of alumina deposits are characterized by much more angular features compared to nickel-chromium deposits. The striations evident in the speci-

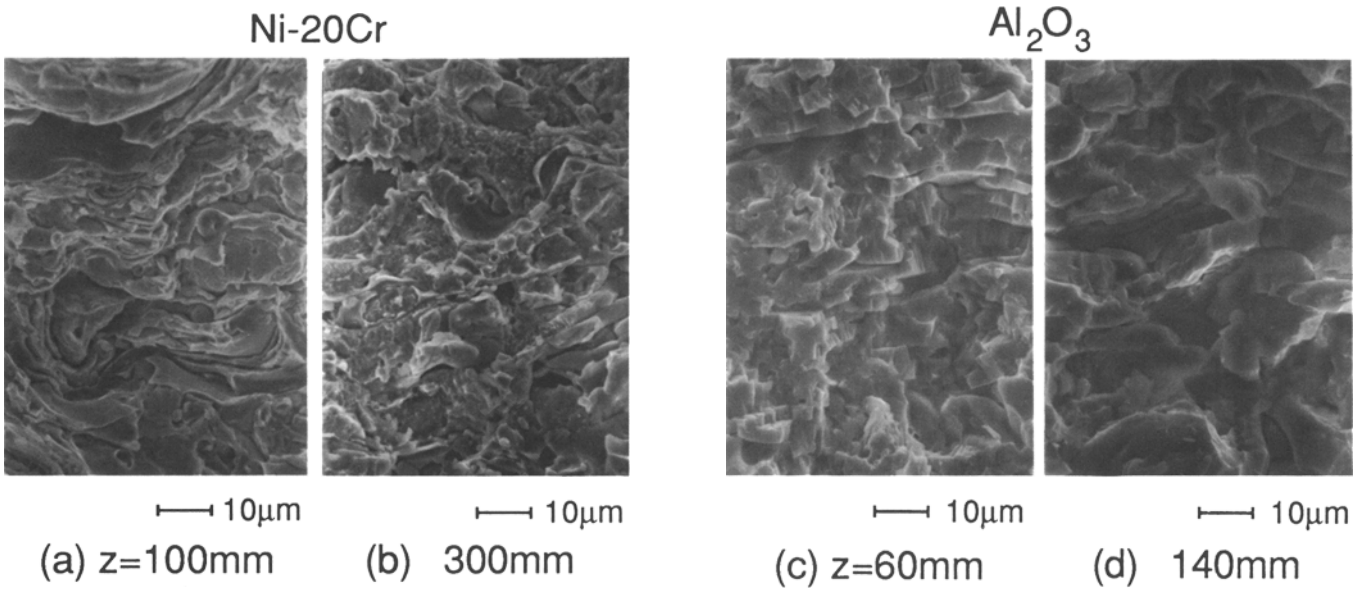

Figure 10 SEM observation of fracture surface orthogonal to the substrate surface of sprayed deposits formed at various spray distances. Ni-20Cr: **(a)** z = 100 mm, **(b)** 300 mm. Alumina: **(c)** z = 60 mm, **(d)** 140 mm.

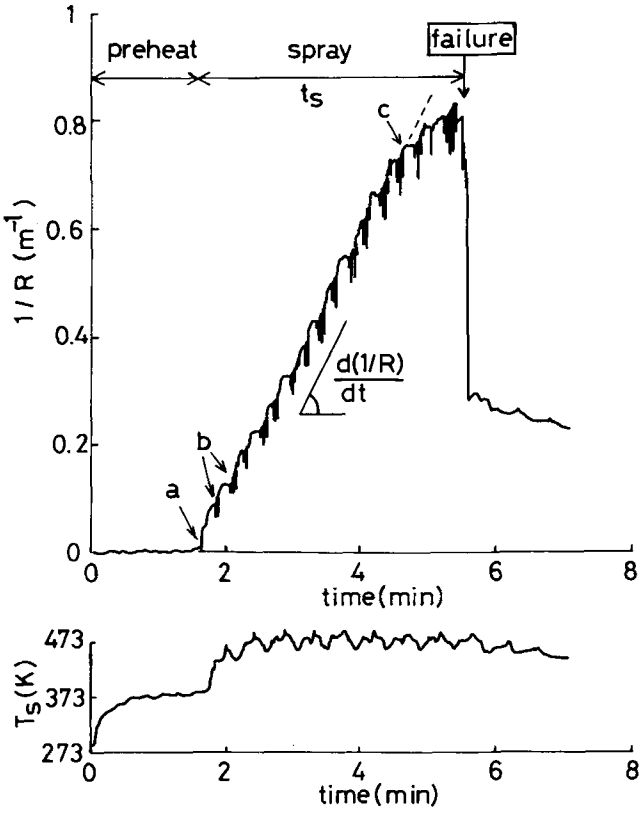

Figure 11 Typical curvature change $1/R$ during spraying Ni-20Cr at z = 100 mm with a record of the substrate temperature, T_s.

men formed at z = 60 mm (Fig. 10c) probably correspond to a columnar crystal structure. Figure 10(d), formed at z = 140 mm, shows a coarser structure with thicker lamellae, which agrees with the observations of splats described earlier (*i.e.*, Fig. 7d).

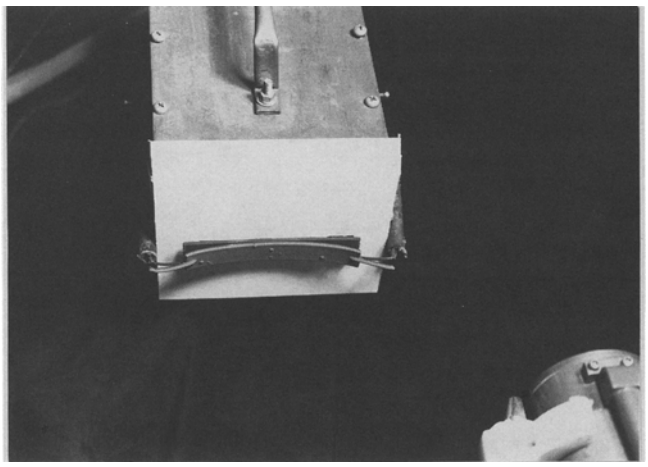

Figure 12 View of *in situ* curvature instrument with a Ni-20Cr coating spontaneously peeling off during spraying due to the high quenching stress of the material.

3.3 *Curvature and Stress*

Figure 11 shows a typical example of the change in curvature of a substrate when Ni-20Cr is sprayed at z = 100 mm. As soon as spraying is started after preheating, the sprayed surface starts to bend concave at point a. The small periodic fluctuations at, for example, point b observed in $1/R$ are due to the transient thermal gradient mainly from the heat of incoming powder.[4,6] By neglecting the small fluctuations in the $1/R$ trace and approximating it by a straight line, one can calculate the slope $d(1/R)/dt$ as shown in Fig. 11. The average growth rate dh_d/dt of the coating is calculated by dividing the final coating thickness h_d by the spraying time t_s. Then $d(1/R)/dh_d$ is calculated and substituted into Eq 2 to give the average quenching stress σ_q. As $1/R$ exceeds

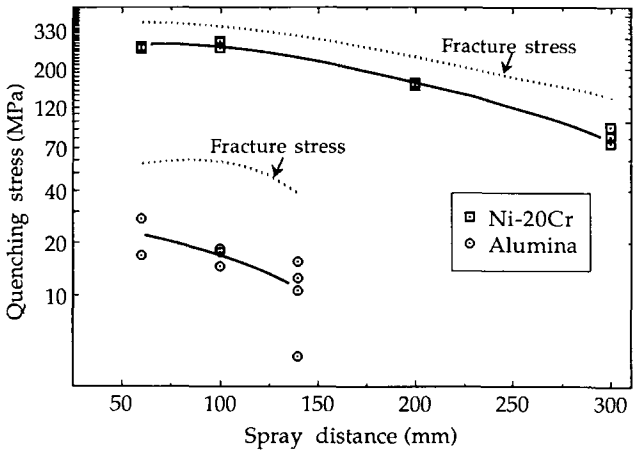

Figure 13 Dependence of quenching stress, σ_q, on the spray distance, z, with fracture stress of the deposits shown by the dotted curves.

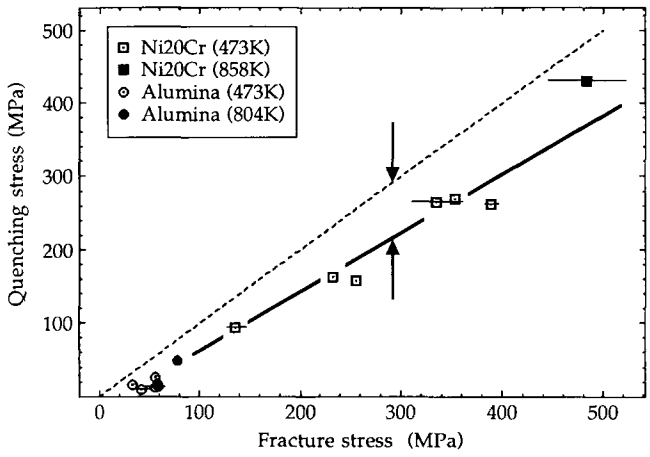

Figure 14 Correlation between quenching stress, σ_q, and fracture stress.

a certain value at point c, its rate of increase gradually decreases and finally falls suddenly, which indicates the initiation of failure at the coating/substrate interface. The following crack propagation leads to delamination of the coating. Figure 12 shows an example of a Ni-20Cr coating spontaneously peeling off during spraying due to its high quenching stress.

Figure 13 shows the dependence of σ_q on the spray distance z. The quenching stress σ_q of nickel-chromium and alumina both decrease with z in general, but the rate of decrease is much greater with alumina. The general tendency with z is very similar to the fracture stress expressed by the dotted curves. Especially for nickel-chromium, the value of σ_q ranges from 50 to 80% of the fracture stress, whereas it ranges from 25 to 40% for alumina.

Values of the strain energy release rate of plasma sprayed deposits have been reported to be significantly lower than the corresponding bulk materials.[14] A double cantilever beam method was used to apply stress orthogonal to the substrate surface. For cohesive interlamellar failure within a coating, the strain energy release rate (G_c) of alumina deposits was about half the value of sintered dense alumina, whereas G_c of sprayed mild steel and NiAl were about an order of magnitude smaller than the bulk material. The moderate reduction in G_c of alumina deposits compared to bulk materials was suggested to be due to crack branching by microcracks, which would enhance the resistance to crack propagation. The drastic reduction in G_c of the metallic deposits compared to the bulk material was attributed to poor interlamellar contact due to entrapped gas and an oxide layer existing between lamellae.[14]

Even though the stress state at interlamellar interfaces in the above-mentioned work is in Mode I (*i.e.*, tensile stress state) whereas that of the present case is in Mode II (*i.e.*, shear stress state), a similar line of discussion may be applicable to the present results. For the Ni-20Cr deposits, the shear strength of interlamellar bonding limits both the quenching stress and the fracture stress, and therefore, those two values are close. For alumina, microcracking is another significant stress relaxation mechanism during quenching that reduces σ_q to the observed low level. It may be because the network of microcracks once formed resists crack propagation that the fracture stress of alumina deposits is higher than σ_q by a factor of more than 2.

Such a discussion is limited, and further understanding of the nature of interlamellar bonding is clearly needed; for example, the area of true contact, the structure of the interlamellar boundary, effects of residual stresses, and effects of oxide layers to facilitate more quantitative analysis. Nevertheless, the general similarity in the dependence of stiffness, strength, and quenching stress on the spray distance seems to indicate that they are limited by the same variables as discussed above in the low-temperature region.

In Fig. 14, the values of σ_q in Fig. 13 are replotted against the values of the fracture stress at the corresponding spray distance, and their correlation can be seen more clearly. Several data points obtained from specimens prepared on a relatively hot substrate (but not hot enough for σ_q of Ni-20Cr to be reduced due to creep and yielding) placed at z = 100 mm also conform to this relation. The figure also indicates that these as-deposited coatings are already highly stressed, and the margin in the tensile side indicated by a pair of arrows is rather narrow. Therefore, if the coating is put into further tension by thermal stress during cooling after deposition or by external stress under various loading conditions during service, it is likely to crack at a significantly lower stress level than would be expected from the intrinsic strength of the coating.

4. Conclusion

The general sensitivity of mechanical properties of sprayed deposits to the spray distance reflects the change in the temperature and velocity of sprayed powders. Modulus and strength of alumina deposits are much more sensitive to the spray distance compared to those of Ni-20Cr deposits. The behavior of the quenching stress with respect to the spray distance is similar to that of the modulus and strength in the low-temperature range. It suggests that the strength of interlamellar bonding and the size and distribution of microcracks are critically important to all these properties. There is a possibility to use the *in situ* curvature measurement as a convenient tool to examine the reasons for

coating failure during deposition, because it can quantify the stress within a coating and the onset of coating delamination in a single experiment.

Acknowledgments

Mr. H. Itoh of Nihon University is acknowledged for his sincere cooperation in many of the experiments. We are also grateful to Mr. Y. Isoda and Y. Tamura of NRIM for their technical assistance in SEM analysis.

References

1. S. Kuroda and T.W. Clyne, The Quenching Stress in Thermally Sprayed Coatings, *Thin Solid Films*, Vol 200, 1991, p 49-66.
2. S. Kuroda and T.W. Clyne, The Origin and Quantification of the Quenching Stress Associated with Splat Cooling during Spray Deposition, *Proc. 2nd Plasma-Technik Symp.*, Vol 3, S. Blum-Sandmeier, H. Eschnauer, P. Huber, and A.R. Nicoll, Ed., Plasma-Technik AG, Wohlen, Switzerland, 1991, p 273-283.
3. S.C. Gill and T.W. Clyne, Stress Distributions and Material Response in Thermal Spraying of Metallic and Ceramic Deposits, *Metall. Trans. B*, Vol 21, 1990, p 377-385.
4. S.C. Gill and T.W. Clyne, Thermomechanical Modelling of the Development of Residual Stresses during Thermal Spraying, *Proc. 2nd Plasma-Technik Symp.*, Vol 3, S. Blum-Sandmeier, H. Eschnauer, P. Huber, and A.R. Nicoll, Ed., Plasma-Technik AG, Wohlen, Switzerland, 1991, p 227-237.
5. S.J. Howard and T.W. Clyne, Measurement and Control of the Interfacial Fracture Toughness of Plasma Sprayed Coatings, *Proc. 2nd Plasma-Technik Symp.*, Vol 3, S. Blum-Sandmeier, H. Eschnauer, P. Huber, and A.R. Nicoll, Ed., Plasma-Technik AG, Wohlen, Switzerland, 1991, p 249-261.
6. S. Kuroda, T. Fukushima, and S. Kitahara, Generation Mechanisms of Residual Stresses in Plasma-Sprayed Coatings, *Vacuum*, Vol 41 (No. 4-6), 1990, p 1297-1299.
7. S. Kuroda, T. Fukushima, S. Kitahara, H. Fujimori, Y. Tomita, and T. Hiriuchi, Monitoring of Thermally Sprayed Particles using Thermal Radiation, Paper No. 27, *12th Int. Conf. Thermal Spraying*, I.A. Bucklow, Ed., The Welding Institute, Abington, UK, 1989.
8. G. Stoney, The Tension of Metallic Films deposited by Electrolysis, *Proc. Roy. Soc. London*, Vol A82, 1909, p 172-175.
9. S. Kuroda, T. Fukushima, and S. Kitahara, Simultaneous Measurement of Coating Thickness and Deposition Stress during Thermal Spraying, *Thin Solid Films*, Vol 164, 1988, p 157-163.
10. A. Brenner and S. Senderoff, Calculation of Stress in Electrodeposits from the Curvature of a Plated Strip, *J. Res. Nat. Bur. Stand.*, Vol 42, 1949, p 105-123.
11. W.D. Nix, Mechanical Properties of Thin Films, *Metall. Trans. A*, Vol 20, 1989, p 2217-2245.
12. R.McPherson and B. Shafer, Interlamellar Contact within Plasma-Sprayed Coatings, *Thin Solid Films*, Vol 97, 1982, p 201-204.
13. A. Ohmori and C.-J. Li, Quantitative Characterization of the Structure of Plasma-Sprayed Al_2O_3 Coating by using Copper Electroplating, *Thin Solid Films*, Vol 201, 1991, p 241-252.
14. R. McPherson, The Relationship between the Mechanism of Formation, Microstructure and Properties of Plasma-Sprayed Coatings, *Thin Solid Films*, Vol 83, 1981, p 297-1310.